Liquid Crystals
Publication details, including instructions for authors and subscription information:
http://www.informaworld.com/smpp/title~content=t713926090

Change of the lateral chain conformation in the solid and the nematic phase in laterally substituted nematogens

F. Perez[a]; P. Berdagué[a]; P. Judeinstein[a]; J. P. Bayle[a]; H. Allouchi[b]; D. Chasseau[b]; M. Cotrait[b]; E. Lafontaine
[a] Laboratoire de Chimie Structurale Organique, Université Paris XI, Orsay Cedex, France [b] Laboratoire de Cristallographie et Physique Cristalline, Université Bordeaux I, Talence Cedex, France

To cite this Article Perez, F. , Berdagué, P. , Judeinstein, P. , Bayle, J. P. , Allouchi, H. , Chasseau, D. , Cotrait, M. and Lafontaine, E.(1995) 'Change of the lateral chain conformation in the solid and the nematic phase in laterally substituted nematogens', Liquid Crystals, 19: 3, 345 — 352
To link to this Article: DOI: 10.1080/02678299508031991
URL: http://dx.doi.org/10.1080/02678299508031991

LIQUID CRYSTALS, 1995, VOL. 19, NO. 3, 345–352

Change of the lateral chain conformation in the solid and the nematic phase in laterally substituted nematogens

by F. PEREZ, P. BERDAGUÉ, P. JUDEINSTEIN, J. P. BAYLE*
Laboratoire de Chimie Structurale Organique. URA 1384 CNRS, Bât. 410,
Université Paris XI. 91405 Orsay Cedex, France

H. ALLOUCHI, D. CHASSEAU, M. COTRAIT
Laboratoire de Cristallographie et Physique Cristalline. ERS 133 CNRS,
351, Cours de la Libération, Université Bordeaux I. 33405 Talence Cedex, France

and E. LAFONTAINE
DGA/CREA, 16 bis Avenue Prieur de la Côte d'Or. 91414 Arcueil Cedex, France

(*Received 27 January 1995; accepted 31 March 1995*)

A new homologous series of 4-(4′-ethoxybenzoyloxy)-2-alkoxy-4′-(4-butoxysalicylaldimine)-azobenzenes has been synthesized. These compounds contain four rings in the main core and a lateral alkoxy branch on one of the inner rings and present enantiotropic nematic properties. The X-ray crystal structure (MoK_α radiation, $\lambda = 0{\cdot}7071$ Å, graphite monochromator) of 4-(4′-ethoxybenzoyloxy)-2-butoxy-4′-(4-butoxysalicylaldimine)azobenzene was investigated ($T = 293$ K, $R = 0{\cdot}059$ for the 2855 observed reflections). This compound ($C_{36}H_{39}N_3O_6$) crystallizes in the monoclinic system with C2/c space group; ($Z = 8$); $a = 28{\cdot}052(7)$ Å, $b = 7{\cdot}545(4)$ Å, $c = 33{\cdot}823(7)$ Å and $\beta = 112{\cdot}70(1)°$. There is a strong chelated hydrogen bond between the OH group and the neighbouring nitrogen atom engaged in the imine bridge. In the solid state, the molecule is roughly linear with a 31 Å length. The lateral butoxy chain is quasi-perpendicular to the long axis of the main core. The crystal cohesion is due to numerous Van der Waals interactions. At the solid to nematic transition, a change in the conformation of the lateral chain occurs from an all *trans*-conformation to one involving a *cis*-conformation in the first part of the lateral chain. This change can be monitored by the evolution of the ^{13}C chemical shift of the OCH_2 belonging to the lateral alkoxy chain.

1. Introduction

Laterally substituted mesogens are of considerable interest because these compounds deviate from the classical rod-like shape. It has been shown that flexible lateral substituents do not destroy the ordering of liquid crystalline phases [1, 2]. In fact, a strong decrease in the melting and clearing temperatures for the first members of a series is observed. However, as the chain length increases, the effect of the additional perturbation diminishes, and chains with three or more carbons perturb the molecular arrangement in the liquid crystalline phase to a similar extent. It was pointed out in several studies that, because every additional carbon only slightly perturbs the liquid crystal ordering, the lateral flexible substituent probably adopts a special conformation and is oriented along the molecular long axis [3, 8]. If the mesogenic core is sufficiently rigid and contains four aromatic rings, we have shown that a large nematic range can be obtained [9]. Recently, we have used one-dimensional ^{13}C NMR and a two-dimensional NMR method called separated local field (SLF) with a BLEW-48 homonuclear decoupling sequence to study the orientational ordering of some liquid crystals with a similar structure [10]. We found that the value of the order parameter of the inner aromatic ring indicates that the molecular long axis is nearly aligned with the *para*-axis of this fragment. The lateral alkoxy chain does not play an important role in influencing the position of the long axis as the main core is fairly large. This chain was found to align in the nematic field created by the four ring system. In addition, the results suggested that the first three-carbon fragment of the lateral chain adopts a *cis*-conformation allowing the chain to be aligned along the main core. The problem of the conformation change of the lateral chain between the solid phase and the liquid crystal phase is then of interest.

In this paper, we present the synthesis of some new

* Author for correspondence.

0267–8292/95 $10·00

laterally substituted compounds, the X-ray crystal structure of one of these compounds and the ^{13}C solid state spectra of two of these compounds in order to examine the behaviour of the lateral chain when going from the solid to the nematic phase.

2. Experimental

2.1. *Synthesis*

The compounds were prepared according to the scheme shown in figure 1 and the detailed procedure is given in [9].

The synthesis of the monoalkylated resorcinols involved the use of a mixture of polyethylene glycol (MW = 200) and dioxane (25:75) as solvent and potassium hydrogen carbonate as base [11]. The coupling with the monodiazotised 4-phenylenediamine was carried out in the same solvent mixture. Then, the amine was purified by chromatography with chloroform as eluent. The Schiffs base was obtained using conventional methods [12, 13]. The compounds **A** containing two hydroxyl groups were crystallized from chloroform/acetonitrile. In the last step, the selective esterification was effected in dichloromethane using the dicyclohexylcarbodiimide (DCC) method [14]. The ethoxybenzoic acid was added slightly in excess, in order to consume the Schiffs base totally. The compounds **B** were purified by several recrystallizations from toluene/ethanol (30/70) until constant transition temperatures were obtained. The compounds are referred to as AL*n* where *n* is the number of carbons in the lateral chain.

The structures and the purity of the compounds were checked by ^1H NMR using an AM 250 Bruker spectrometer and by an R10-10C Nermag mass spectrometer.

2.2. *DSC measurements*

The phase transitions were observed and characterized by using an Olympus polarizing microscope fitted with an FP 82 Mettler heating stage and by using an FP 85 Mettler DSC without prior melting of the samples. The transition temperatures obtained were recorded at a 10°C min^{-1} heating rate.

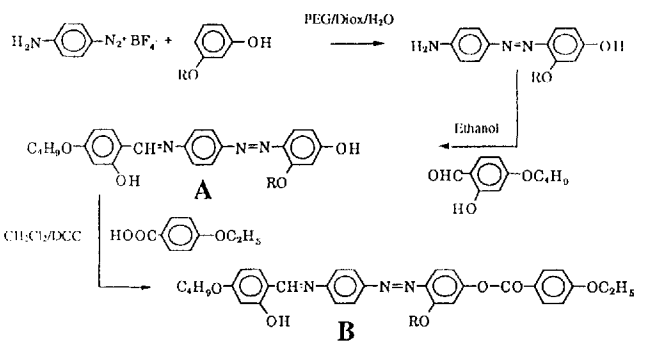

Figure 1 Synthetic scheme for 4-(4′-ethoxybenzoyloxy)-2-alkoxy-4′-(4-butoxysalicylaldimine)azobenzenes.

2.3. *X-ray data collection and structure resolution*

Suitable crystals of AL4 were grown from $CHCl_3$ solution at 293 K. The crystal setting, the cell parameters and the data collection were obtained with an Enraf-Nonius diffractometer, equipped with a graphite monochromator (MoK_α radiation; $\lambda = 0{\cdot}7071$ Å). 25 reflections with θ between 9 and 14° were used for the crystal setting and least-squares refinement of the cell parameters: $a = 28{\cdot}052(7)$ Å, $b = 7{\cdot}545(4)$ Å, $c = 33{\cdot}823(7)$ Å, $\beta = 112{\cdot}70(1)°$, $V = 6604$ Å^3, $d_c = 1{\cdot}226$ g cm^{-3}, $F(000) = 2592$ and $\mu = 0{\cdot}91$ cm^{-1}, monoclinic system and C2/c space group ($Z = 8$).

The scan width and the detector aperture during data collection were, respectively, equal to $(3{\cdot}0 + 2{\cdot}5 \tan\theta)°$ and $(1{\cdot}7 + 0{\cdot}35 \tan\theta)$ mm, using $\omega - 2\theta$ scans; $\theta < 25°$ ($-32 < h < 32$, $0 < k < 8$, $-38 < l < 38$), so that each reflection was measured twice. There was no significant decrease in the reference reflections; minimum and maximum transmission factors were 0·98 and 1·0, so that no correction of absorption was necessary. 7230 reflections were measured, out of which 4119 were independent ($R_{int} = 0{\cdot}94$ per cent). Finally only 2825 independent reflections were considered as observed ($I > 3\,\sigma(I)$).

The structure was solved by direct methods, using the MITHRIL package [15], which led to the position of almost all non-hydrogen atoms; the remaining atoms appeared after successive Fourier syntheses. The terminal butyl chain is disordered, and this leads to two different positions of the carbon atoms, with an occupancy factor of 0·5.

Atomic parameters for non-hydrogen atoms were refined anisotropically by full-matrix least-squares using SHELX76 [16]; H-atoms were located in their theoretical positions [17] and constrained to follow the displacements of the carbon atoms to which they are linked. The weighting scheme was $w = 1{\cdot}0/(\sigma(F)^2 + 0{\cdot}000365\,F^2)$; scattering factors were taken from International Tables for X-ray Crystallography (1974, Tome IV). The final reliability factors were $R = 0{\cdot}059$ and $wR = 0{\cdot}074$; $(\Delta/\sigma)\max = 0{\cdot}15$ and the residual electronic density ρ is between $-0{\cdot}2$ and $0{\cdot}5$ eÅ^{-3}.

2.4. *C-13 spectra in the solid and nematic phase*

High-resolution ^{13}C NMR experiments were performed with a Bruker MSL 200 spectrometer with quadrature detection using a double-tuned coil for ^{13}C and ^1H NMR. The samples were placed in fused zirconia rotors fitted with boron nitride caps and spun at 6 kHz at the magic angle (54·7°). ^{13}C chemical shifts were referenced to the

glycine carbonyl signal (assigned at 176·03 ppm) used as external reference. The spectra were obtained using cross-polarization pulsing (with a ^{1}H 90° pulse of 4·1 μs), high power decoupling during acquisition, 0·03 s acquisition, 3 s recycle delay, 512 scans and 1·2 ms mixing time. Variable temperature CP/MAS NMR experiments were performed in the 30–150°C range using a Eurotherm controller, calibrated for the DABCO (1,4-diazabicyclo(2,2,2)octane) crystal–crystal transition [18].

3. Results and discussion

3.1. *DSC measurements*

The transition temperatures of the compounds are given in table 1. All compounds gave enantiotropic nematic phases with large liquid crystalline ranges. It should be noted that the first members of the series have poor thermal stability above the melting temperature. Table 2 gives the entropies associated with the phase transitions. The entropy change at the nematic–isotropic temperature $\Delta S_{NI}/R$ falls with the number of carbons in the lateral chain. This trend has been previously observed for nematogens having a lateral chain [8]. Figure 2 shows the dependence of the transition temperatures on the number of carbon atoms (n) in the lateral alkoxy chain. The decrease in T_{NI} (nematic–isotropic transition) is rather smooth and we do not observe a limiting value in T_{NI} as observed for other series of nematogens with lateral chains [8]. This may be due to the relatively short lateral chain compared to the large mesogenic core. T_{CrN} (crystal–nematic transition) shows an inflection for two

Table 1. Transition temperatures (in °C) of the 4-(4′-ethoxybenzoyloxy)-2-alkoxy-4′-(4-butoxysalicylaldimine)azobenzenes series. The heating rate was 10°C min^{-1}.

n	Cr_1	→	Cr_2	→	N	→	I
2			157		289		
4			158		267		
6	149		153		257		
8	99		130		247		
10	85·5		106·5		234·5		
12	106·5		126		221·5		

Table 2. Entropies of transition for the 4-(4′-ethoxybenzoyloxy)-2-alkoxy-4′-(4-butoxysalicylaldimine)azobenzenes.

n	$\Delta S_{CrCr}/R$	$\Delta S_{CrN}/R$	$\Delta S_{NI}/R$
2		12·8	0·68
4		11·8	0·54
6	2·6	10·0	0·46
8	1·1	13·4	0·39
10	1·6	11·4	0·38
12	2·2	15·4	0·32

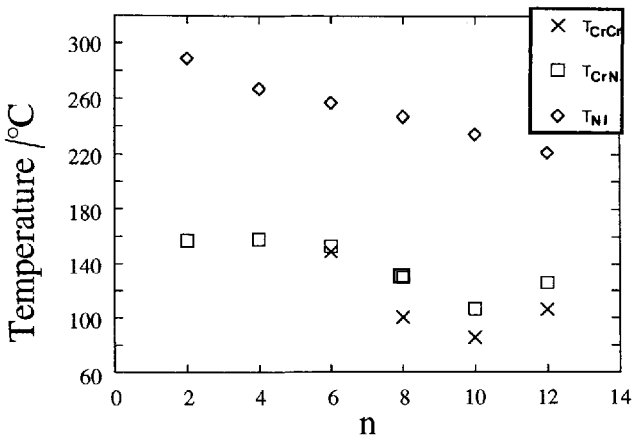

Figure 2. Phase behaviour for the homologous series of compounds **B** (ALn), where n is the number of carbons in the lateral chain.

lateral chains containing 6 carbons. This inflection corresponds to the appearance of solid–solid phase transitions in the series. Some DSC plots of AL8 are presented in figure 3. The first curve was recorded with a 10°C min^{-1} heating rate without prior melting of the sample; a clear solid–solid phase transition is observed at 99°C (see figure 3 (*a*)). When the sample is heated up to 120°C and then cooled down to room temperature, a second heating run gives the solid–solid phase transition nearly at the same temperature (98°C) (see figure 3 (*b*)). When the sample is heated into the nematic or isotropic phase, then, after cooling down, the solid–solid transition in a new heating run rises by 15°C and sharpens (see figure 3 (*c*)). On the contrary, the solid–nematic and nematic–isotropic transitions are not affected by the

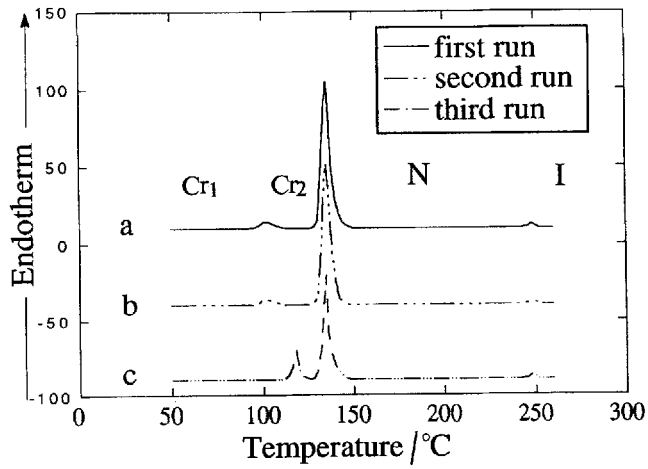

Figure 3. DSC traces for AL8 from room temperature to the clearing temperature as obtained with different thermal histories of the sample. First run (*a*): no prior heating: second run (*b*): prior heating up to 120°C: third run (*c*): prior heating up to 160°C.

cycling of the sample. These differences in the DSC curves indicate that the solid-state structure is changed by thermal treatment. As the solid–solid transition occurs with long lateral chains, it should be emphasized that the structural change involves the far part of this chain as discussed in the NMR section.

3.2. *X-ray analysis*

The fractional coordinates *x/a*, *y/b*, *z/c* and the U_{eq} (Å^2) temperature factors are given in table 3; the U_{eq} values of disordered carbon atoms (C360 ... C395) belonging to the terminal butyl chain are particularly high. For the sake of clarity, the drawing with the thermal ellipsoids is not presented and only a ball-and-stick representation is shown in figure 4 [19]. Selected bond distances and angles are given in tables 4 and 5.

The four aromatic rings are designed as φ_1 (atoms C1 to C6), φ_2 (atoms C20 to C25), φ_3 (atoms C30 to C35) and φ_4 (atoms C40 to C45); they are perfectly planar. All the atoms (C7, N8, N9, N10, O16, C18, O19, O26 and O29) directly linked to a ring are in the mean plane of this ring. The φ_1/φ_2, φ_1/φ_3 and φ_2/φ_3 dihedral angles are, respectively, 12·9°, 1·5° and 14·4°, and the corresponding torsion angles are close to 180° within a 20° range. These results give an idea of the strong conjugation between these three aromatic rings. On the contrary, the φ_1/φ_4, φ_2/φ_4 and φ_3/φ_4 dihedral angles are, respectively, equal to 51·6°, 64·4° and 50·1°, and the torsion angle around O16–C33 is equal to − 115·3° due to the large deviation (1·06 Å) of carbon atom C18 from the φ_3 plane. This indicates the poor conjugation induced by the carboxyl group.

The molecule is roughly linear with a length (C28 ... C390) close to 31 Å. The terminal chain (O29 to C390) and the lateral butoxy chain (O11 to C15) are planar and stretched with, respectively, 4·46 Å and 4·87 Å lengths. It should be noticed that the lateral chain is 10 per cent longer than the terminal one. The angle between the main chain (O26 ... O29) and the lateral butoxy chain (O11 to C15), which is in the φ_3 plane, is close to 77°. The C3 atom belonging to the φ_1 aromatic ring bears an OH group. An intramolecular hydrogen bond O19–H119 ... N8 is found with distances N8 ... O19 and N8 ... H119, respectively, equal to 2·60 and 1·96 Å, and an angle N8 ... H119–O19 equal to 151°.

The molecules are aligned along the *a* axis and are quasi-parallel to the *x*O*z* plane (4°). The projection of the structure along the *b* axis is presented in figure 5. The molecules have no longer a rod-like shape in the solid phase, due to the nearly perpendicular lateral chain. This molecular conformation induces the molecules to make a very complex network in the solid. Interactions between neighbouring molecules are very weak and the distances very close to the sum of the Van der Waals radii. The crystal cohesion must be due to the sum of these weak interactions. The absence of short range interactions with the terminal butoxy chain might explain the rather high thermal motion of these atoms and their disordered character.

Table 3. Atomic coordinates ($\times 10^4$) and equivalent isotropic thermal parameters *U*eq (Å^2) ($\times 10^3$ Å^2), where *U*eq (Å^2) = 1/3 $\Sigma_i\Sigma_j a_i^* a_j^* \mathbf{a_i a_j}$ for AL4.

Atom	*x/a*	*y/b*	*z/c*	*U*eq
C1	8617(2)	1398(7)	5890(2)	90(7)
C2	8116(2)	1791(7)	5610(2)	83(6)
C3	7717(2)	1599(7)	5746(2)	74(6)
C4	7808(2)	1038(6)	6166(2)	64(5)
C5	8316(2)	681(7)	6438(2)	81(6)
C6	8725(2)	863(8)	6309(2)	88(6)
C7	7391(2)	846(6)	6307(2)	65(5)
N8	6923(1)	1193(5)	6072(1)	64(4)
N9	5257(1)	423(5)	6593(1)	66(24)
N10	4831(1)	942(6)	6333(1)	67(4)
O11	3901(1)	1503(5)	5764(1)	80(4)
C12	3406(2)	1879(7)	5434(1)	67(5)
C13	3507(2)	2399(8)	5044(2)	82(6)
C14	3011(2)	2995(8)	4688(2)	90(6)
C15	3095(2)	3574(9)	4288(2)	109(7)
O16	3108(1)	261(4)	6755(1)	69(3)
O17	3370(1)	2436(5)	7237(1)	104(5)
C18	3042(2)	1405(7)	7042(2)	63(5)
O19	7237(2)	1964(6)	5464(1)	97(5)
C20	6520(2)	976(6)	6221(1)	58(5)
C21	6040(2)	1695(7)	5963(1)	68(5)
C22	5615(2)	1554(7)	6076(2)	67(5)
C23	5669(2)	682(6)	6447(1)	58(5)
C24	6138(2)	− 27(6)	6706(2)	71(5)
C25	6559(2)	108(6)	6591(2)	72(5)
O26	1167(1)	982(4)	7252(1)	73(4)
C27	753(2)	− 99(8)	7000(2)	98(7)
C28	345(2)	52(10)	7177(3)	158(9)
O29	9010(2)	1568(6)	5752(2)	148(6)
C30	4414(2)	694(7)	6468(2)	64(5)
C31	3923(2)	1052(6)	6160(1)	62(5)
C32	3493(2)	902(6)	6265(1)	61(5)
C33	3563(2)	415(6)	6676(2)	65(5)
C34	4035(2)	37(7)	6979(2)	75(5)
C35	4458(2)	179(7)	6871(2)	75(5)
C360	9497(4)	1100(18)	5956(4)	121(10)
C365	9022(5)	2287(22)	5404(5)	180(12)
C370	9739(6)	1678(26)	5623(5)	176(11)
C375	9594(5)	2862(19)	5428(5)	146(12)
C380	10301(8)	1795(33)	5686(7)	366(14)
C385	9865(5)	1156(23)	5512(6)	200(12)
C390	10261(8)	2715(23)	5276(7)	239(12)
C395	10385(9)	1419(39)	5434(12)	399(14)
C40	2540(2)	1188(6)	7072(1)	49(4)
C41	2126(2)	253(6)	6782(1)	55(5)
C42	1662(2)	150(6)	6830(1)	56(5)
C43	1606(2)	980(6)	7176(1)	54(5)
C44	2011(2)	1914(6)	7467(1)	56(5)
C45	2474(2)	2036(6)	7416(1)	56(5)
H119	7043(16)	1823(51)	5617(14)	84(14)

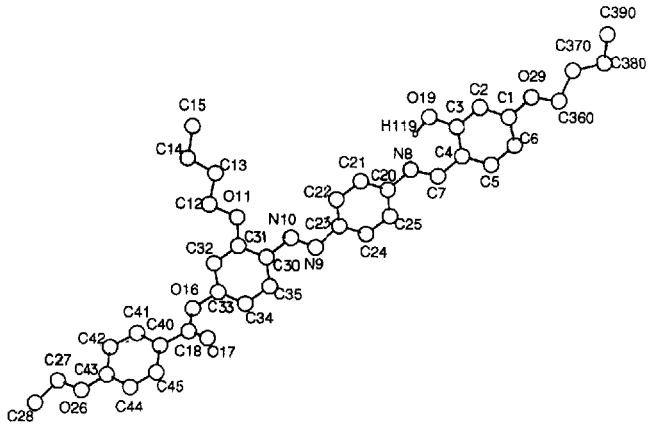

Figure 4. X-ray structure of AL4 and atomic numbering.

Table 4. Bond lengths (Å), with standard deviations, for AL4.

Bond	Length	Bond	Length
C1–C2	1·391 (9)	C23–C24	1·376 (7)
C1–C6	1·391 (9)	C23–C24	1·376 (7)
C1–O29	1·359 (8)	C24–C25	1·383 (7)
C2–C3	1·371 (8)	O26–C27	1·407 (7)
C3–C4	1·410 (7)	O26–C43	1·351 (6)
C3–O19	1·344 (7)	C27–C28	1·486 (9)
C4–C5	1·391 (7)	O29–C360	1·317 (13)
C4–C7	1·431 (7)	O29–C365	1·308 (16)
C5–C6	1·383 (8)	C30–C31	1·395 (7)
C7–N8	1·273 (7)	C30–C35	1·376 (7)
N8–C20	1·415 (6)	C31–C32	1·386 (7)
N9–N10	1·243 (6)	C32–C33	1·375 (6)
N9–C23	1·434 (6)	C33–C34	1·356 (7)
N10–C30	1·422 (6)	C34–C35	1·376 (7)
O11–C12	1·436 (5)	C360–C370	1·586 (21)
O11–C31	1·360 (5)	C365–C375	1·631 (22)
C12–C13	1·504 (7)	C370–C380	1·510 (29)
C13–C14	1·514 (7)	C375–C385	1·466 (23)
C14–C15	1·524 (8)	C380–C390	1·515 (30)
O16–C18	1·364 (6)	C385–C395	1·592 (34)
O16–C33	1·404 (6)	C40–C41	1·389 (6)
O17–C18	1·191 (6)	C40–C45	1·401 (6)
C18–C40	1·461 (7)	C41–C42	1·376 (7)
C20–C21	1·401 (7)	C42–C43	1·390 (6)
C20–C25	1·378 (7)	C43–C44	1·376 (6)
C21–C22	1·387 (7)	C44–C45	1·378 (7)
C22–C23	1·373 (7)	O19–H119	0·889 (46)

3.3. ^{13}C *spectra in the solid and nematic phases*

Due to the temperature probe limitation, it was not possible to reach the clearing temperature of the AL4 sample. Therefore, we will discuss the evolution of the ^{13}C chemical shift for AL8 as this compound exhibits in addition a solid–solid phase transition at 99°C. The proton-decoupled 50 MHz ^{13}C spectrum of AL8 in $CDCl_3$ solution, the MAS spectra of AL8 in the solid and the nematic phases are presented in figure 6.

Table 5. Bond angles (°), with standard deviations, for AL4.

Atoms	Angle	Atoms	Angle
C2–C1–C6	121·4 (6)	C23–C24–C25	120·1 (5)
C2–C1–O29	119·2 (5)	C20–C25–C24	120·9 (5)
C6–C1–O29	119·4 (6)	C27–O26–C43	119·0 (4)
C1–C2–C3	119·4 (5)	O26–C27–C28	107·2 (5)
C2–C3–C4	121·0 (5)	C1–O29–C360	127·5 (7)
C2–C3–O19	117·7 (5)	C1–O29–C365	130·8 (8)
C4–C3–O19	121·3 (5)	N10–C30–C31	115·6 (4)
C3–C4–C5	117·8 (5)	N10–C30–C35	125·7 (4)
C3–C4–C7	120·8 (5)	C31–C30–C35	118·7 (4)
C5–C4–C7	121·4 (5)	O11–C31–C30	116·1 (4)
C4–C5–C6	122·4 (5)	O11–C31–C32	124·0 (4)
C1–C6–C5	118·0 (5)	C30–C31–C32	119·9 (4)
C4–C7–N8	123·4 (5)	C31–C32–C33	118·7 (4)
C7–N8–C20	121·9 (4)	O16–C33–C32	115·3 (4)
N10–N9–C23	113·5 (4)	O16–C33–C34	122·0 (4)
N9–N10–C30	114·8 (4)	C32–C33–C34	122·6 (5)
C12–O11–C31	118·5 (4)	C33–C34–C35	118·2 (5)
O11–C12–C13	106·3 (4)	C30–C35–C34	121·9 (5)
C12–C13–C14	110·5 (4)	O29–C360–C370	101·3 (10)
C13–C14–C15	112·5 (5)	O29–C365–C375	115·5 (12)
C18–O16–C33	117·7 (4)	C360–C370–C380	128·8 (15)
O16–C18–O17	121·4 (5)	C365–C375–C385	101·7 (12)
O16–C18–C40	112·3 (4)	C370–C380–C390	101·1 (17)
O17–C18–C40	126·4 (5)	C375–C385–C395	107·4 (17)
C3–O19–H119	103·5 (28)	C18–C40–C41	124·9 (4)
N8–C20–C21	116·2 (4)	C18–C40–C45	116·6 (4)
N8–C20–C25	125·7 (4)	C41–C40–C45	118·5 (4)
C21–C20–C25	118·1 (4)	C40–C41–C42	121·1 (4)
C20–C21–C22	121·3 (4)	C41–C42–C43	119·6 (4)
C21–C22–C23	119·0 (5)	O26–C43–C42	124·6 (4)
N9–C23–C22	124·1 (4)	O26–C43–C44	115·1 (4)
N9–C23–C24	115·2 (4)	C42–C43–C44	120·3 (4)
C22–C23–C24	120·7 (4)	C43–C44–C45	120·1 (4)
		C40–C45–C44	120·5 (4)

The two MAS spectra were obtained without any prior melting of the sample. In the solid state spectra, all the lines are reasonably sharp, but in the aromatic and aliphatic part of the spectra, we observed an overlapping of the different signals except for the OCH_2 signals. In the OCH_2 region in the solid phase, we observed two peaks; the one at 69 ppm is double in intensity and corresponds to the terminal OC4 and the lateral OC8, and the one at 63 ppm corresponds to the terminal OC2. This enforces the idea that the terminal OC4 and the lateral OC8 chains must experience a similar environment. This means that these two chains in AL8 are in an all *trans*-conformation in the solid phase, as for AL4 (see table 6). The different chemical shift of the OCH_2 belonging to the terminal OC2 chain is due to the effect of the terminal methyl group bonded to the OCH_2 fragment. Figure 7 gives the evolution of the chemical shifts as a function of temperature for the OCH_2 carbons in the solid and nematic phases.

At the solid–solid phase transition, the evolution of the chemical shift is small, indicating that the transition does

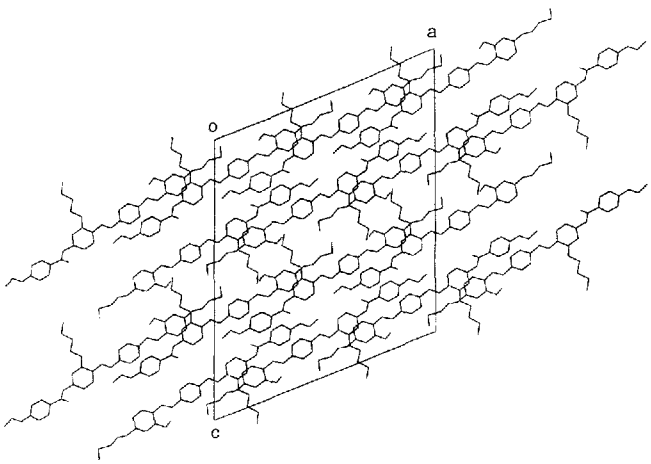

Figure 5. Projection of the crystal structure along the *y* axis for AL4.

not affect to a large extent the conformations of these carbons. Furthermore, the aliphatic part below 30 ppm changes to a large extent, indicating that the solid–solid transition may involve the melting of the far part of the lateral chain. At the solid–nematic transition, the double OCH_2 line splits into two peaks. The one assigned to the OCH_2 of the lateral chain shifts downfield remarkably by 1·8 ppm from that just before the melting point, while the OCH_2 of the terminal OC4 chain shows an upfield shift of 1·2 ppm. These chemical shifts are obtained at the magic angle and do not contain any contribution from the orientational order. They can be compared to those obtained in solution, as they are nearly independent of the solvent. We found that the two OCH_2 belonging to the terminal chains have similar chemical shifts. On the contrary, a 1·5 ppm downfield shift is observed for the signal of the OCH_2 borne by the lateral chain (see table 5). Usually, in mesogens bearing a terminal alkoxy chain, the C_β, C_γ and C_δ resonances show a downfield shift from solution to the solid phase, while the C_α resonance is less affected [20–23]. These chemical shift differences are interpreted on the basis of the γ-*gauche* effect [24, 25]. The γ-*gauche* shielding parameters are dependent on the dihedral angle in the C_α–C_β–C_γ–C_δ fragment. Resonances of aliphatic carbons shift upfield by about 5 ppm when the conformation changes from *trans* (180°) to *gauche* (60°). In the solid state, a terminal alkoxy group is locked in an all *trans*-conformation and is free of γ-*gauche* effect. In solution, the chemical shift is averaged over all the conformations. Some are in a γ-*gauche* conformation which induces upfield shifts up to 4 ppm. This is clearly shown in figure 7 for the two terminal OCH_2, if we note that the chemical shifts in solution and in the nematic phase are nearly the same.

On the contrary, the OCH_2 of the lateral chain shows a noticeable upfield shift in the solid phase and a downfield

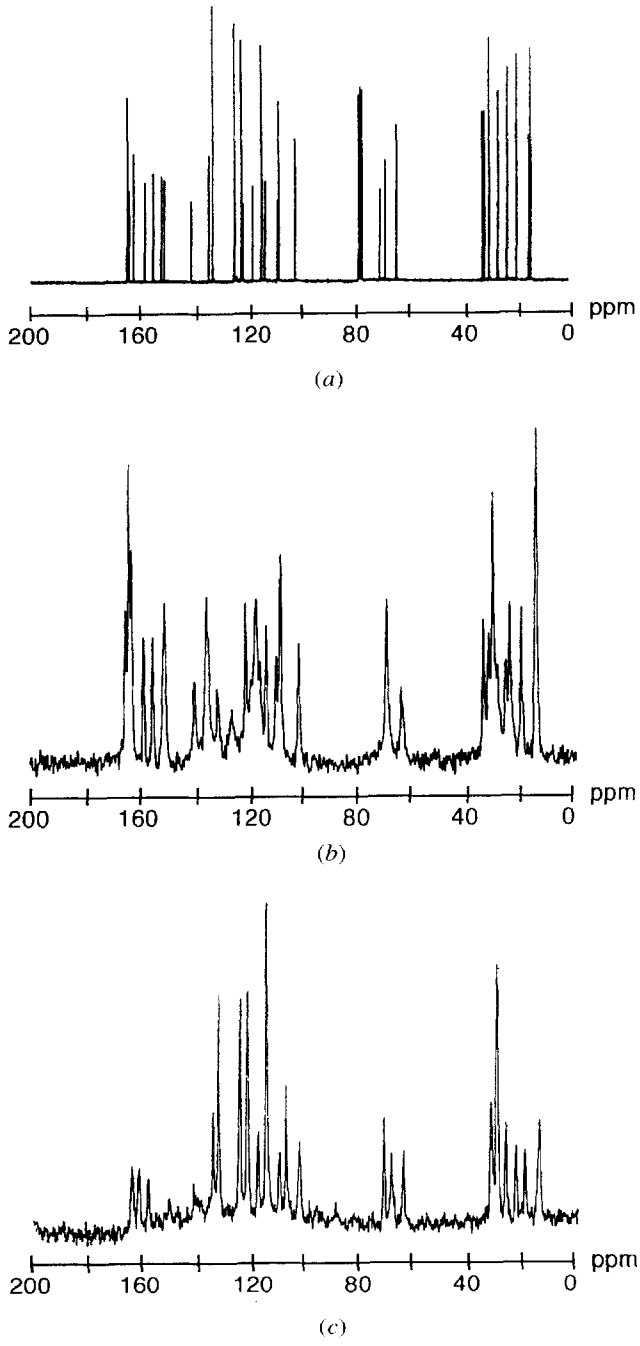

Figure 6. 50 MHz proton dipolar decoupled ^{13}C NMR spectra of AL8. (*a*): in $CDCl_3$ solution; (*b*): in the solid phase; (*c*): in the nematic phase.

shift in the nematic phase by comparison with the isotropic chemical shift. The resonance frequency of this carbon is deshielded by 2 ppm compared to the *trans*-arrangement in the solid. This shift is opposite to the one induced by a γ-*gauche* conformation. In order to evaluate the lateral chain conformation and its effect on the chemical shifts, we have performed energy calculations on some conformations with the idea of obtaining a low-energy

Table 6. ^{13}C chemical shifts for compounds AL4 and AL8, in the solid state and in solution, and for AL8 in the nematic phase. Some assignments might be interchanged.

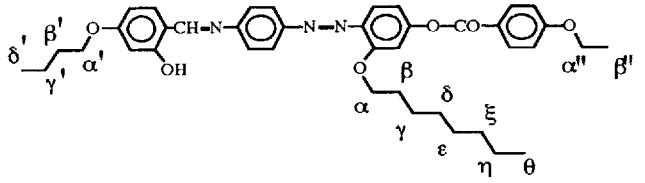

AL8 lateral chain	α	β	γ	δ	ε	ξ	η	θ
Solution ($CDCl_3$)	69·8	31·7	26·0	29·2	29·2	29·1	22·6	14·0
Solution (C_6D_6)	69·7	32·1	26·3	29·7	29·5	29·5	23·0	14·3
Solid (298 K)	68·7	33·5	25·9	29·9	29·9	31·7	23·8	14·2
Nematic (408 K)	71·1	31·7	26·4	29·6	29·6	29·6	22·7	13·9
AL8 terminal chains	α'	β'	γ'	δ'	α''	β''		
Solution ($CDCl_3$)	67·9	31·0	19·7	13·7	63·7	14·6		
Solution (C_6D_6)	67·9	31·3	19·4	13·9	63·6	14·5		
Solid (298 K)	68·7	31·6	19·7	14·2	63·4	14·2		
Nematic (408 K)	68·4	29·6	19·3	13·9	63·9	13·9		
AL4 lateral chain	α	β	γ	δ				
Solution ($CDCl_3$)	69·4	31·1	19·2	13·8				
Solution (C_6D_6)	69·3	31·5	19·5	13·8				
Solid (300 K)	68·5	32·7	19·6	13·8				
AL4 terminal chains	α'	β'	γ'	δ'	α''	β''		
Solution ($CDCl_3$)	67·9	31·0	19·1	13·7	63·7	14·5		
Solution (C_6D_6)	67·8	31·3	19·4	14·0	63·6	14·5		
Solid (300 K)	67·8	32·7	19·6	14·9	64·2	16·0		

conformation with the lowest free space between the lateral substituent and the main core (Nemesis Program; Oxford Molecular Ltd. 1992). It was found that the main core was fairly planar. The lateral alkoxy chain was assumed to lie in the same plane as the main core; a *cis*-conformation involving the first carbon was then obtained (see figure 8). In the nematic phase, the chain adopts many conformations and the observed chemical shift results from the weighted sum of the chemical shifts of all these conformations, but the appearance of a liquid crystalline phase suggests the crude assumption that the conformation in which the lateral chain is aligned along the mesogenic core (see figure 8) is predominant. In this conformation, the OCH_2 group lies in the nodal plane of the neighbouring azo group. Then, the resonance of the carbon can be affected by the deshielding effect of the azo group due to ring current anisotropy. In the liquid crystalline phase, the existence of the nematic field increases the population of this conformation. In solution, this population is depleted and then the effect on the chemical shift is diminished.

4. Conclusions

In this paper, we have presented the synthesis and properties of some compounds containing four rings in the main core and two terminal alkoxy chains containing 2 and 4 carbons and substituted by a different lateral alkoxy chain in one of the inner rings. These compounds have a large enantiotropic nematic range. The crystal structure of AL4 indicates that the three aromatic rings linked by the imine and the azolinks are in the same plane, which gives an idea of the strong conjugation between these three aromatic rings. The terminal alkoxy chains and the lateral chain are also planar and stretched with lengths of 4·46 Å and 4·87 Å, respectively. The molecule is roughly linear with a length close to 31 Å. The conformation of the lateral chain is all-*trans* and its orientation is quasi-perpendicular to those belonging to the main core. The DSC and MAS spectra of AL4 and AL8 indicate that the chain conformation of the first carbons does not evolve from the solid phase. On the contrary, at the solid–nematic transition, the lateral chain conformation changes from all-*trans* to a conformation involving the *cis*-conformation

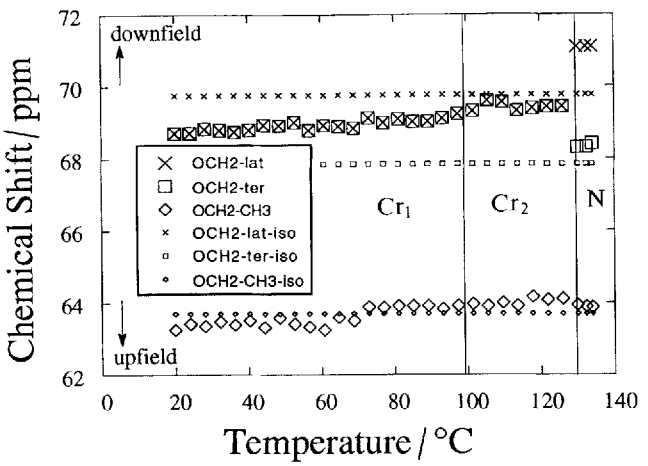

Figure 7. Chemical shift dependence of the lateral OCH_2 carbons of AL8 on increasing the temperature. The horizontal lines indicate the isotropic chemical shift of these carbons obtained for a $CDCl_3$ solution.

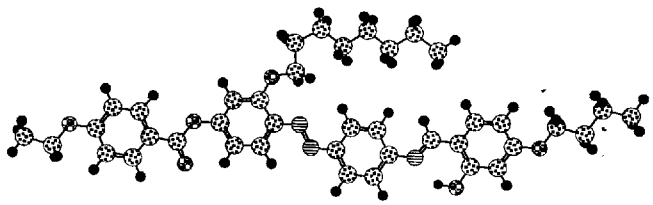

Figure 8. Mean energy minimized molecular conformation of AL8 in the nematic phase.

in the first carbon fragment. Other results on molecules with one or two lateral alkoxy chains will be published separately.

References

[1] WEISSFLOG, W., and DEMUS, D., 1983, *Crystal Res. Tech.*, **18,** K21.
[2] WEISSFLOG, W., and DEMUS, D., 1984, *Crystal Res. Tech.*, **19,** 55.
[3] WEISSFLOG, W., and DEMUS, D., 1985, *Molec. Crystals liq. Crystals*, **129,** 235.
[4] DEMUS, D., 1989, *Liq. Crystals*, **5,** 75.
[5] ATTARD, G. S., and IMRIE, C. T., 1989, *Liq. Crystals*, **6,** 387.
[6] NGUYEN, H. T., and DESTRADE, C., 1989, *Molec. Crystals liq. Crystals Lett.*, **6,** 123.
[7] BALLAUF, M., 1987, *Liq. Crystals*, **2,** 519.
[8] IMRIE, C. T., and TAYLOR, L., 1989, *Liq. Crystals*, **6,** 1.
[9] BERDAGUÉ, P., PEREZ, F., JUDEINSTEIN, P., and BAYLE, J. P., 1995, *New J. Chem.*, **19,** 293.
[10] BERDAGUÉ, P., PEREZ, F., BAYLE, J. P., HO MEI-SING, and FUNG, B. M., 1995, *New. J. Chem.*, **19,** 383.
[11] BERDAGUÉ, P., PEREZ, F., COURTIEU, J., and BAYLE, J. P., 1993, *Bull. Soc. Chim. Fr.*, **130,** 475.
[12] BUI, E., BAYLE, J. P., PEREZ, F., and COURTIEU, J., 1991, *Bull. Soc. Chim. Fr.*, **127,** 61.
[13] BERDAGUÉ, P., PEREZ, F., COURTIEU, J., and BAYLE, J. P., 1994, *Bull. Soc. Chim. Fr.*, **131,** 335.
[14] HASSNER, A., and ALEXANIAN, V., 1978, *Tetrahedron Lett.*, **46,** 4475.
[15] GILMORE, C. J., 1984, *J. appl. Cryst.*, **17,** 42.
[16] SHELDRICK, G. M., 1976, *SHELX76, Program for Crystal Structure Determination*, University of Cambridge, England.
[17] LEHMAN, H. S., KOETSEL, T. F., and HAMILTON, W. C., 1972, *J. Am. chem. Soc.*, **94,** 2657.
[18] HAW, J. F., 1988, *Analytical Chem.*, **559,** A60.
[19] DAVIES, K., 1983, *SNOOPI, Program for Drawing Crystal and Molecular Diagrams*, Chemical Laboratory, University of Oxford, England.
[20] OULYADI, H., LAUPRÊTRE, F., MONNERIE, L., MAUZAC, M., RICHARD, H., and GASPAROUX, H., 1990, *Macromolecules*, **23,** 1965.
[21] KATO, T., FUJISHIMA, A., URYU, T., MATSUSHITA, N., and YAMAGUCHI, H., 1990, *New Polymeric Mater.*, **2,** 255.
[22] KATO, T., and URYU, T., 1987, *Molec. Crystals liq. Crystals Lett.*, **5,** 17.
[23] KATO, T., and URYU, T., 1991, *Molec. Crystals liq. Crystals.* **195,** 1.
[24] TONELLI, A. E., and SCHILLLING, F. C., 1981, *Acc. Chem. Res.*, **14,** 233.
[25] TONELLI, A. E., 1991, *Macromolecules*, **24,** 3065.